JOURNAL OF OPTOELECTRONICS AND ADVANCED MATERIALS Vol. 8, No. 1, February 2006, p. 355 - 358

Top mirror optimization of high-speed intracavity - contacted oxide-confined vertical-cavity surface - emitting lasers

V. V. LYSAK[a,b*], KI SOO CHANG[a], YONG TAK LEE[a]
[a]*Department of Information and Communications, Gwangju Institute of Science and Technology (GIST), 1 Oryong-dong, Buk-ku, Gwangju, 500-712, Republic of Korea*
[b]*Laboratory "Photonics", Kharkov National University of Radio Electronics, 14, Lenin av., Kharkov, 61166, Ukraine*

This work presents the simulation of the intra-cavity contacted oxide vertical confined cavity surface emitting lasers (VCSEL) including the thermal effects. The analysis of thermal, electrical and optical properties of these devices is carried out for different top mirror radii. The results show that the optimal relation between the top mirror and oxide window radii of device is 1.3-1.5.

(Received June 1, 2005; accepted January 26, 2006)

Keywords: DC characteristics, Intracavity contacted oxide confined vertical cavity surface emitting laser, Modulation bandwidth

1. Introduction

Over short distances inside computer systems or clusters of electronic networks, board-to-board or chip-to-chip multi gigahertz bandwidth optical interconnects are required to replace electrical interconnects. The optical interconnects include direct interconnects among boards, arbitrary interconnection patterns, multiple fanouts, channel isolation, and increased bandwidth, thus, avoiding the interconnection bandwidth bottleneck of systems with strictly in-plane electronic interconnects. In communications and computer-related fields, the fusion of electrical and optical technologies has progressed rapidly. Pushing performance levels even higher will soon require hybrid circuit boards that integrate optical chips alongside electrical chips. An important key to creating these hybrid integrated optoelectronic circuit boards is the alignment between the optical chips and the optical waveguides on the circuit boards. Optical interconnects can be found in an increasing number of applications involving high data rate and/or real time operations such as a short distance network, computer, and signal processing board [1]. Vertical-Cavity Surface-Emitting Lasers (VCSELs) is a useful light source that can be applied to chip-to-chip and board-to-board optical data link with bandwidths greater than 10 GHz, which are expected to play a key role for these next-generation network transceivers [2].

The edge emitting lasers can divide the VCSELs into two classes: index and gain guided. Index guided structures confine the current and optical mode using an etched pillar structure, [3] which lights in predictable transverse modes determined by the wave guide dimensions. The gain guided structures use the proton implantation [4] or oxidized [5] layer to confine the region of current injection. In gain guided structures thermal lensing and spatial hole burning effects are important on the transverse mode profile due to the lack of strong index discontinuities.

By the place of contacts VCSELs can be divided on extra-cavity (EC) and intra-cavity (IC) contacted structures. In first case, the carrier is injected into the active region by passing through the distributed Bragg reflector (DBR) mirror stack [6]. In order to reduce the driving voltage and improve their power conversion efficiency the DBR resistance is decreased by grading the interfaces and making the complex doping profiles that increase the optical losses [6]. In the intra-cavity-contacted VCSELs the active region is bordered by two highly doped contact layers to inject current and the substrate and DBR remain undoped to minimize optical losses [7]. The intra-cavity contacted oxide confined VCSELs (ICOC-VCSELs) with dielectric top mirror stack are presented for wavelength of 980 nm (MgF/ZnSe mirror) [2] and 850 nm (SiO_2/TiO_2 mirror) [8], respectively. Using the dielectric mirrors allows receiving the appropriate reflectivity at 6 periods of alternating layers, but the additional fabrication processes should be included that increase a cost of device.

We will show that the more detailed analysis of device's geometrical parameters adding to previously published improvements (asymmetrical contact layers for counter-flowing currents [2] and graded-doped p-contact for suppressing the current crowding effect and decrease of the free carrier absorption loss [9]) allows receiving the 10 GHz modulation bandwidth for structures with standard AlAGAs/GaAs DBR mirrors, which are more useful for devices that can be fabricated with low cost compatible processes of conventional printed circuit board.

The modulation properties of VCSEL can be predicted by the relaxation resonance. For bias currents, sufficiently far above threshold to ensure effective carrier clamping, the frequency of this resonance is given by [10]:

$$f_R = \frac{1}{2\pi}\sqrt{\eta_i \frac{\Gamma v_g}{qV} g'(I - I_{th})} \qquad (1)$$

where η_i is the internal quantum efficiency; Γ is the confinement factor; q is the electron charge; V is the effective volume of resonator including the penetration depth of DBR mirrors; g' is the differential gain; I is the bias current and I_{th} is the threshold current. On the other hand, the resonant frequency can be determined by RC parasitic by [11]:

$$f_R \sim (R_{tot} C_{par})^{-0.5} \tag{2}$$

where R_{tot} is the total device resistance and C_{par} is the parasitic capacitance.

The geometrical parameters that can be optimized to improve the modulation properties of ICOC VCSEL are following: the oxide window diameter, relation between the top mirror and oxide window radii of device, contact layer thickness, the thickness of graded layer at contact layer – oxide window interface. The basic analysis shows on one hand, at increasing of each parameter value the volume of the resonator is increased. On other hand, at decreasing of parameter value the device resistance is increased. These both processes allow decreasing the resonant frequency (see equations (1) and (2)). If the resonant frequency decreases in both direction of change of top mirror radius, there is some optimal region with the maximum of modulation bandwidth.

In this paper we consider the influence of relation between the top mirror and oxide window radii on device's CW and modulation characteristics. Other parameters will be analyzed in next publications.

2. Structure description

The schematic representation of 980 nm ICOC VCSEL is shown in Fig. 1. The active layer contains two 80 Å $In_{0.2}Ga_{0.8}As$ quantum wells (QWs), 150 Å GaAs barrier between the 200 Å SCH barriers. Resonator contains the two 1100 Å $Al_{0.42}Ga_{0.58}As$ cladding layers. The thickness of p- and n-contact layers is 2088 Å. The p – contact layer is divided on two parts with different doping concentration (696 Å with doping concentration 4×10^{18} cm^{-3} and 1392 Å with doping concentration 2×10^{18} cm^{-3}) to suppress the current crowding effect and decrease the free carrier absorption loss [9]. The 100 Å thickness graded layer is included at contact layer-oxide window aperture interface to decrease the resistance between the layers and improve the driving voltage of device. The width of the contacts is 10 μm and the diameter of oxide window aperture is 12 μm. The top and bottom Bragg reflector stacks consist of 25 $Al_{0.9}Ga_{0.1}As$/GaAs and 27 AlAs/GaAs layer pairs, respectively.

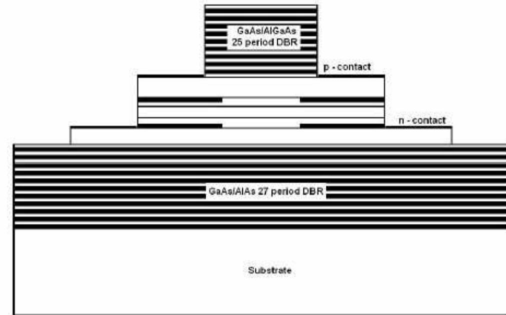

Fig. 1. ICOC-VCSEL structure.

3. Numerical simulations and description of results

The theoretical model of IC VCSEL including the optical, thermal and electrical properties was analyzed in [12]. But in this model the main effects like temperature effect, spatial hole burning and optical field distribution are considered by simple analytical formulations. Additionally the n-contact layer was treated as a ground plain that did not fully describe the current flowing. In our case the self-consistent modelling of electrical, optical and thermal properties is used [13]. This model simulates wide spectrum characteristics with very large updating possibilities of new material parameters and calculation algorithms. Carrier transport is simulated using the drift-diffusion model [14,15]. Calculations of the optical gain, refractive index and spontaneous recombination as a function of wavelength are based on $4\times4\vec{k}\cdot\vec{\mathbf{p}}$ band structure computations for the strained quantum wells. The heat flux equation is included to address self-heating effects. All important heat sources, i.e. nonradiative recombination, absorption of spontaneous radiation as well as volume and Joule heating, are taken into account. The enhanced effective index method [16] is employed for optical simulation including temperature effects on layer thickness, absorption, and refractive index. The lateral optical modes are given by Bessel functions. The main material parameters can be found in literature [17].

Fig. 2 shows the light-current (L-I) and voltage-current (V-I) characteristics for device with oxide window radius is equal to 6 μm and for different values of top DBR mirror radius.

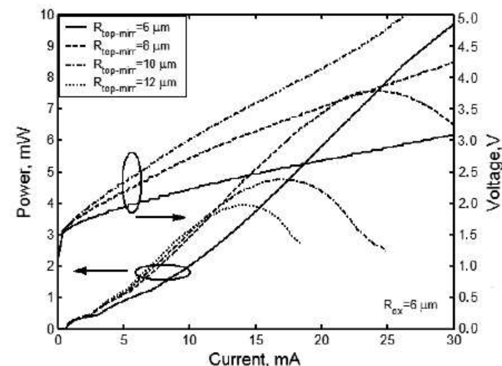

Fig. 2. L-I and V-I characteristics for different top mirror radiuses.

At decreasing the radius of the top mirror the current spreading effect decreases. It allows to larger no uniformity of current distribution in the active region and smaller slope efficiency.

The radial distributions of the electron concentration for devices with radii of top mirror of 6 μm (solid lines) and 10 μm (dashed lines) and for different currents are presented in Fig. 3.

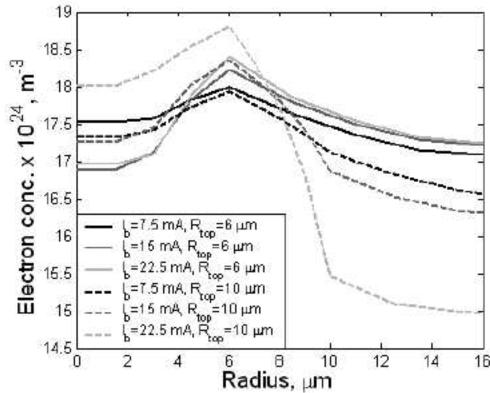

Fig. 3. Radial distribution of electron concentration.

The maxima of curves are placed at the oxide window edge due to current crowding effect. The current crowding problem is much known in bipolar transistors. At low current levels, the device resistance is limited by the diode resistance and so the current injection is relatively uniform. As the diode driven harder, its dynamic resistance becomes very low which shunts the lateral currents in the contacting layer. The additional current is primarily injected around the perimeter [12].

At the center of device electron concentration decreases initially with increasing of the bias current. But after the concentration decreases slightly for the 6 μm top mirror device and decreases large for 10 μm top mirror device due to larger lattice temperature in the active region, which allows decreasing the stimulation recombination rate.

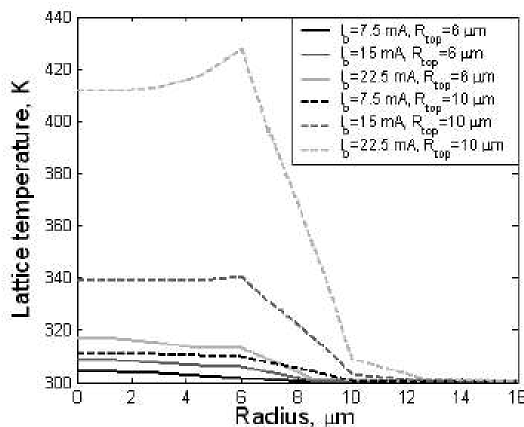

Fig. 4. Radial distribution of the lattice temperature in the active region.

Besides that, the power saturates at smaller currents for device with larger radius of the top mirror (see L-I characteristics in the Fig. 2) due to higher temperature in the active layer.

The radial distribution of the lattice temperature in the quantum well is presented in the Fig. 4. It can be seen the larger increasing of the lattice temperature in the active for the device with larger radius of top mirror.

It can be explained by two facts. Firstly, at increasing the top mirror radius, the horizontal current path between the contact and oxide window region is increased logarithmically [18]. It allows increasing the total resistance of device (see V-I characteristics in Fig. 2) and further increasing the lattice temperature in the centre of device. Secondly, some part of acceptors is located around the perimeter of the top mirror due to diffusion. These acceptors create the region with effective cooling on the side of the top mirror [19]. At increasing the top mirror radius, the distance between this region and the active layer is increased that also allows increasing the temperature in the active layer.

Fig. 5 shows the modulation response of devices with different top mirror radii at pumping current of 10 mA. At the decreasing the top mirror radius, the slope efficiency of L-I characteristics that connected to differential gain is decreased (see L-I characteristics in the Fig. 2). On the other hand, at increasing top mirror radius, the differential resistance (see V-I characteristics in the Fig. 2) is also increased. Fig. 5 shows the maximum bandwidth has a structure with top mirror radius equal to 8μm.

So, the optimal relation between top mirror and oxide window radii $R_{top_ox} = R_{top_mirr} / R_{ox_win} = 1.3{\sim}1.5$ and such devices have the largest modulation bandwidth.

Results on the Fig. 5 show quite small modulation bandwidth of 1.85 GHz, because of using the cylindrical symmetry in our simulation. Using the asymmetrical contact layers the overlap area between p-doped and n-doped regions surrounding the active layers can be decreased that allows decreasing the device capacitance. Furthermore, the holes and electrons were forced to follow equivalent counter-flowing paths throughout the entire aperture that alleviates the current crowding effects by equalizing the lengths of all current paths through the active region of VCSEL [2].

Additionally, the n-contact can be shifted closer to active layer that also allows decreasing the resistance of device.

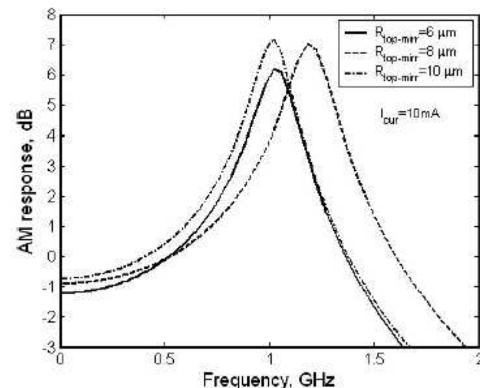

Fig. 5. Modulation response of ICOC VCSELs with different top mirror radii.

4. Conclusions

In this work the thermal, electrical, optical and modulation properties of ICOC VCSELs with different top mirror radii are analyzed. The results of calculation of the light - current characteristic show, from one hand, increasing of the slope efficiency of L-I characteristic with increasing the radius of the top mirror due to current spreading effect. From other hand, the maximal power is smaller for device with larger radius of the top mirror, due to larger lattice temperature in the active region. The modulation characteristics show that the devices with the ratio between the top mirror and oxide window radii of about 1.3-1.5 have the maximum of the modulation bandwidth.

Acknowledgement

This work is supported by Korean Ministry of Education through the BK21 Program and by Korean Ministry of Science and Technology through the National Program for Tera-Level Nano Devices.

References

[1] K.-M. Chu, J.-S. Lee, H.-S. Cho, H.-H Park, D.-Y. Jeon, IEEE Trans. on Electronics packaging manufacturing **27**, 246 (2004).
[2] A. V. Krishnamoorthy, IEEE Photon. Technol. Lett. **12** (2000) 609.
[3] J. L. Jewell, Electron. Lett. **25** (1989) 1123.
[4] K. L. Lear, IEEE Photon. Technol. Lett. **6**, 1053 (1994).
[5] G. M. Yang, Electron. Lett. **31** (1995) 886.
[6] K. L. Lear, IEEE Photon. Technol. Lett. **5**, 972 (1993).
[7] J. W. Scatt, IEEE Photon. Technol. Lett. **6**, 678 (1994).
[8] G. Dang, IEEE Photon. Technol. Lett. **13** (2001) 924.
[9] M. H. McDougal, IEEE J. Select. Topics Quantum Electron. **3** (1997) 905.
[10] Vertical cavity surface emitting lasers: design, fabrication, characterization, and application/ Eds. Carl Wilmsen, Henryk Temkin and Larry A. Coldren, 455 p. Cambridge University Press, 1999.
[11] J. Katz, IEEE J. Quantum Electron. **17** (1981) 4.
[12] J. W. Scatt, IEEE J. Quantum Electron. **29** (1993) 1295.
[13] PICS3D, User's manual and reference manual, version 2002.2, Crosslight Inc., 2002.
[14] S. M. SZE, Physics of semiconductor devices, 2nd edition (Wiley, New York, 1981), Chap. 1-7, p. 279.
[15] I. A. Sukhoivanov, Optical & Quantum Electron. **31**, 997 (1999).
[16] G. R. Hadley, IEEE J. Quantum Electron. **27,** 921 (1991).
[17] J. Piprek, Semiconductor optoelectronics devices. Introduction to physics and simulation (Academic Press, Amsterdam, 2003), p.279
[18] M. H. MacDougal, IEEE Photon. Technol. Lett. **10**, 9 (1998).
[19] V. V. Lysak, Photonics Conference, November 3-5, Danyang, Republic of Korea, T2D2, 2004.

* Corresponding author: Lysak@gist.ac.kr